Collagen matrix remodeling in stented pulmonary arteries after transapical heart valve replacement

Cells
Tissues
Organs

Collagen Matrix Remodeling in Stented Pulmonary Arteries after Transapical Heart Valve Replacement

Samaneh Ghazanfari[a]   Anita Driessen-Mol[a, b]   Simon P. Hoerstrup[c]
Frank P.T. Baaijens[a, b]   Carlijn V.C. Bouten[a, b]

[a]Department of Biomedical Engineering, and [b]Institute for Complex Molecular Systems, Eindhoven University of Technology, Eindhoven, The Netherlands; [c]Regenerative Medicine Program, University Hospital and University of Zurich, Zurich, Switzerland

Abstract

The use of valved stents for minimally invasive replacement of semilunar heart valves is expected to change the extracellular matrix and mechanical function of the native artery and may thus impair long-term functionality of the implant. Here we investigate the impact of the stent on matrix remodeling of the pulmonary artery in a sheep model, focusing on matrix composition and collagen (re)orientation of the host tissue. Ovine native pulmonary arteries were harvested 8 (n = 2), 16 (n = 4) and 24 (n = 2) weeks after transapical implantation of self-expandable stented heart valves. Second harmonic generation (SHG) microscopy was used to assess the collagen (re)orientation of fresh tissue samples. The collagen and elastin content was quantified using biochemical assays. SHG microscopy revealed regional differences in collagen organization in all explants. In the adventitial layer of the arterial wall far distal to the stent (considered as the control tissue), we observed wavy collagen fibers oriented in the circumferential direction. These circumferential fibers were more straightened in the adventitial layer located behind the stent. On the luminal side of the wall behind the stent, collagen fibers were aligned along the stent struts and randomly oriented between the struts. Immediately distal to the stent, however, fibers on both the luminal and the adventitial side of the wall were oriented in the axial direction, demonstrating the stent impact on the collagen structure of surrounding arterial tissues. Collagen orientation patterns did not change with implantation time, and biochemical analyses showed no changes in the trend of collagen and elastin content with implantation time or location of the vascular wall. We hypothesize that the collagen fibers on the adventitial side of the arterial wall and behind the stent straighten in response to the arterial stretch caused by oversizing of the stent. However, the collagen organization on the luminal side suggests that stent-induced remodeling is dominated by contact guidance.

© 2016 S. Karger AG, Basel

Abbreviations used in this paper

ECM	extracellular matrix
SHG	second harmonic generation

Carlijn V.C. Bouten
Department of Biomedical Engineering
Eindhoven University of Technology, De Zaale
NL–5600 MB Eindhoven (The Netherlands)
E-Mail C.V.C.Bouten @ tue.nl

Introduction

Transapical valve implantation is a minimally invasive valve replacement technique on the beating heart for patients with valvular heart disease [Sun et al., 2009]. The combination of this procedure with stented tissue-engineered heart valves provides a low-burden alternative to conventional surgery and may overcome the shortcomings of currently available nonliving heart valve prostheses. Current bioprosthetic and mechanical valve replacements have drawbacks like limited durability or increased risk of coagulation [Hammermeister et al., 2000], but their main limitation for lifelong functionality is their inability to grow, repair and remodel [Hoerstrup et al., 2000; Yacoub and Takkenberg, 2005]. Preclinical evaluation of surgically implanted tissue-engineered heart valves, obtained from autologous cells grown on fast degrading polymer scaffolds, has shown promising results in the past [Hoerstrup et al., 2000]. More recently, the use of stented tissue-engineered valves was evaluated in vivo [Schmidt et al., 2010]. These valves were integrated into a self-expandable stent, crimped for transapical delivery, inserted into the pulmonary artery, and deployed. While the preclinical trials mainly focus on development and function of the valve leaflets, monitoring and optimization of the interaction between the stent and the artery is of equal importance for the success of valved stent implants. Nonphysiological loads induced by the stent may cause undesired arterial responses, such as vascular trauma, neointimal hyperplasia, thrombosis and adverse structural remodeling, compromising the stent-artery interface and long-term functionality of the prosthesis [Post et al., 1994; Rogers et al., 1999; Chung et al., 2002; Willfort-Ehringer et al., 2004]. Optimizing the stent-artery interface requires detailed understanding of the relationship between the mechanical loads and arterial responses, such as remodeling of the extracellular matrix (ECM).

The degree of collagen orientation and the amount of collagen and elastin present in the ECM is of paramount relevance for the mechanical behavior of the artery [Bailey et al., 1998]. Elastin is an important determinant of arterial distensibility and mechanical integrity [Dobrin, 1978]. Collagen is not only involved in load transmission and structural stability but also plays a key role in wound healing [Steed, 1997]. In addition, collagen can change its fiber orientation in response to functional demand changes and mechanical loading of the arterial wall.

Biochemical assays and imaging techniques are essential tools in the follow-up of tissue development for monitoring changes in the composition and structure of the ECM. Second harmonic generation (SHG) is a second-order nonlinear imaging method to visualize anisotropic biological structures lacking a center of symmetry, such as collagen [Georgiou et al., 2000; Campagnola et al., 2002; Zipfel et al., 2003; Strupler et al., 2007]. This technique is preferred to other methods established for collagen observation, like electron microscopy [Eyden and Tzaphlidou, 2001], X-ray diffraction [James et al., 1991] and histological analysis, since it provides high-resolution images with detailed information without photobleaching and extra staining.

Here, we studied the collagen structural remodeling (with SHG) as well as collagen and elastin content (with assays) of the pulmonary artery following the implantation of a stented heart valve in an ovine animal model. The results can be used as inputs for numerical models in the progress toward designing a functional minimally invasive tissue-engineered heart valve implant.

Materials and Methods

Tissue-Engineered Heart Valve and Implantation Procedure
The method of engineering heart valves, including the scaffold preparation, cell and tissue culture, and valve replacement, was previously described by Schmidt et al. [2010]. Briefly, nonwoven polyglycolic acid scaffolds (thickness 1.0 mm; Cellon, Bereldange, Luxemburg) were integrated into self-expandable nitinol stents (length 27 mm, outer diameter 30 mm when fully expanded at 37°C; pfm medical, Cologne, Germany) and seeded with ovine vascular-derived cells (n = 8) using fibrin as a cell carrier [Mol et al., 2005b]. After the valves were cultured for 4 weeks in a diastolic pulse duplicator system [Mol et al., 2005a], they were decellularized using well-established protocols [Spina et al., 2003; Ye et al., 2009]. A main advantage of using a decellularized valve is to avoid valve retraction, which has been shown to be mediated by the cells [van Vlimmeren et al., 2011]. The outer diameter was decreased from 30 to 12 mm for transapical delivery. All animals received human care and the study was approved by the ethics committee [Veterinäramt, Gesundheitsdirektion, Canton Zurich (197/2012)] in compliance with the Guide for the Care and Use of Laboratory Animals, published by the National Institutes of Health (NIH publication No. 85-23). Approximately 30 min before the induction of anesthesia, animals were sedated in their stable with a subcutaneous injection of midazolam (0.5 mg/kg) and buprenorphine (0.01 mg/kg). The animals were then transferred to the preparation room where the neck area was shaved and a venous catheter was placed in the vena jugularis. The anesthesia was induced by intravenous propofol (2–5 mg/kg) so that the animals could be intubated in sternal recumbency. The anesthesia was maintained by spontaneous breathing of 1–3% isoflurane in a 4-liter/min oxygen/air (60:40) combination. The animals were prepared for surgery by shaving the thorax (surgery area) and placing one additional venous and one arterial catheter. Anesthetized animals were then transferred to a nearby operating theater where the anesthesia was

Ghazanfari/Driessen-Mol/Hoerstrup/
Baaijens/Bouten
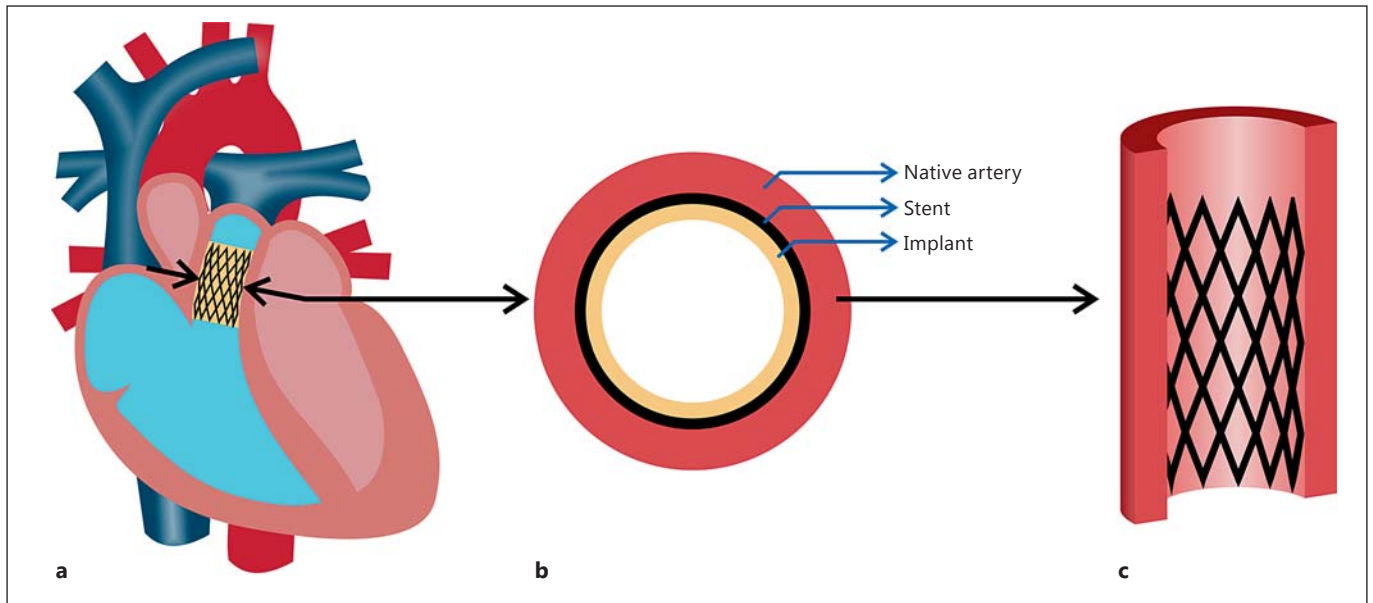
Fig. 1. Schematic view of the tissue-engineered valve in the pulmonary position (**a**), cross-section of the artery (**b**) and the pulmonary artery behind the stent (**c**).

maintained by positive pressure ventilation (7–8 liters/min, 12–15 respirations, max 20 cm H_2O pressure) of 1–3% isoflurane in an oxygen/air (60:40) mixture. To ensure sufficient analgesia during surgery, an additional bolus of buprenorphine (0.01 mg/kg) and caprofen (Rymadil 3 mg/kg) was administered intravenously. Once on a respirator, a neuro-muscular blocking agent was administered (pancuronium bromide, 0.03 mg/kg) to the animals. Furthermore, 1 g of cefazolin was given intravenously for antibiotic prophylaxis. Tetanus serum (3 min, subcutaneous) was also administered. During the whole procedure, animals were monitored by electrocardiography using needle electrodes, invasive blood pressure measurement, pulse oximetry applied to the tongue, lip or shaved ear (whichever provided the best signal) and expired gas analysis for end-tidal carbon dioxide and isoflurane. Pupil size and response, lacrimation, swallowing, shivering and crude assessment of neck muscle tone were used as clinical markers of the depth of anesthesia. The delivery device was inserted into the pulmonary position of the adult sheep and the engineered heart valve deployed out of the delivery device (fig. 1a). When the surgical procedure had finished and the animals were breathing spontaneously, levomethadone (0.05 mg/kg) was administered as an immediate postoperative analgesia. After 8 (n = 2), 16 (n = 4) and 24 weeks (n = 2), the animals were sacrificed and the stented valves were explanted. Native pulmonary artery segments (fig. 1b, c) from 3 different regions (behind the stent, immediately distal to the stent and ~5 cm distal to the stent) were obtained from the fresh explants to evaluate the effect of stenting on the collagen orientation and amount.

Collagen Imaging and Orientation Analysis

A Zeiss LSM 510 Meta laser scanning microscope (Carl Zeiss, Oberkochen, Germany) equipped with an inverted Axiovert 200 motorized microscope (Carl Zeiss) was used to visualize collagen organization. A mode-locked Chameleon Ultra 140-fs pulsed Ti-Sapphire laser (Coherent, Santa Clara, Calif., USA) was tuned to 800 nm and the collagen SHG signal was collected from the sample. All fresh native arteries were scanned at the 3 different locations and from both luminal and adventitial sides. At each location, a stack of 2D images was obtained up to a penetration depth of 100 µm. The distance between two adjacent optical slices was 1 µm. To quantify the collagen orientation on individual images, an algorithm developed in Mathematica (Wolfram, Champaign, Ill., USA) was used [Daniels et al., 2006; Rubbens et al., 2009; Ghazanfari et al., 2012]. Using circular statistics, the mean fiber angle (α), by averaging the angles, and dispersity of the fiber orientations (r) was calculated from the histograms with a 3.5-degree interval obtained from each image. To calculate the mean vector, the decomposed sine and cosine vector components of all unit vectors of the histogram were averaged and to obtain the fiber dispersity (r), the length of the mean vector was calculated. If r was zero, fibers were randomly oriented and if r was 1, fibers were completely aligned [Ghazanfari et al., 2015b]. Fiber angles were calculated with respect to the vertical (Y) or the axial direction of the vessel.

In a previous study, we developed a method to quantify a tortuosity index (as a measure of collagen fiber waviness) in stented tissue-engineered valvular walls. The tortuosity index data of tissue-engineered samples were compared with those of native vascular wall tissue located behind the stent [Ghazanfari et al., 2015a]. In short, the tortuosity index was calculated using a Gabor wavelet method, which varied between 0 and 1. If the tortuosity index was 0, there was no tortuosity, and if the tortuosity index was 1, tortuosity was very high. Using the same method, here we compared the tortuosity index of the native vascular wall behind the stent obtained from the previous study [Ghazanfari et al., 2015a] with the tortuosity index of the native vascular wall located distal to the stent.
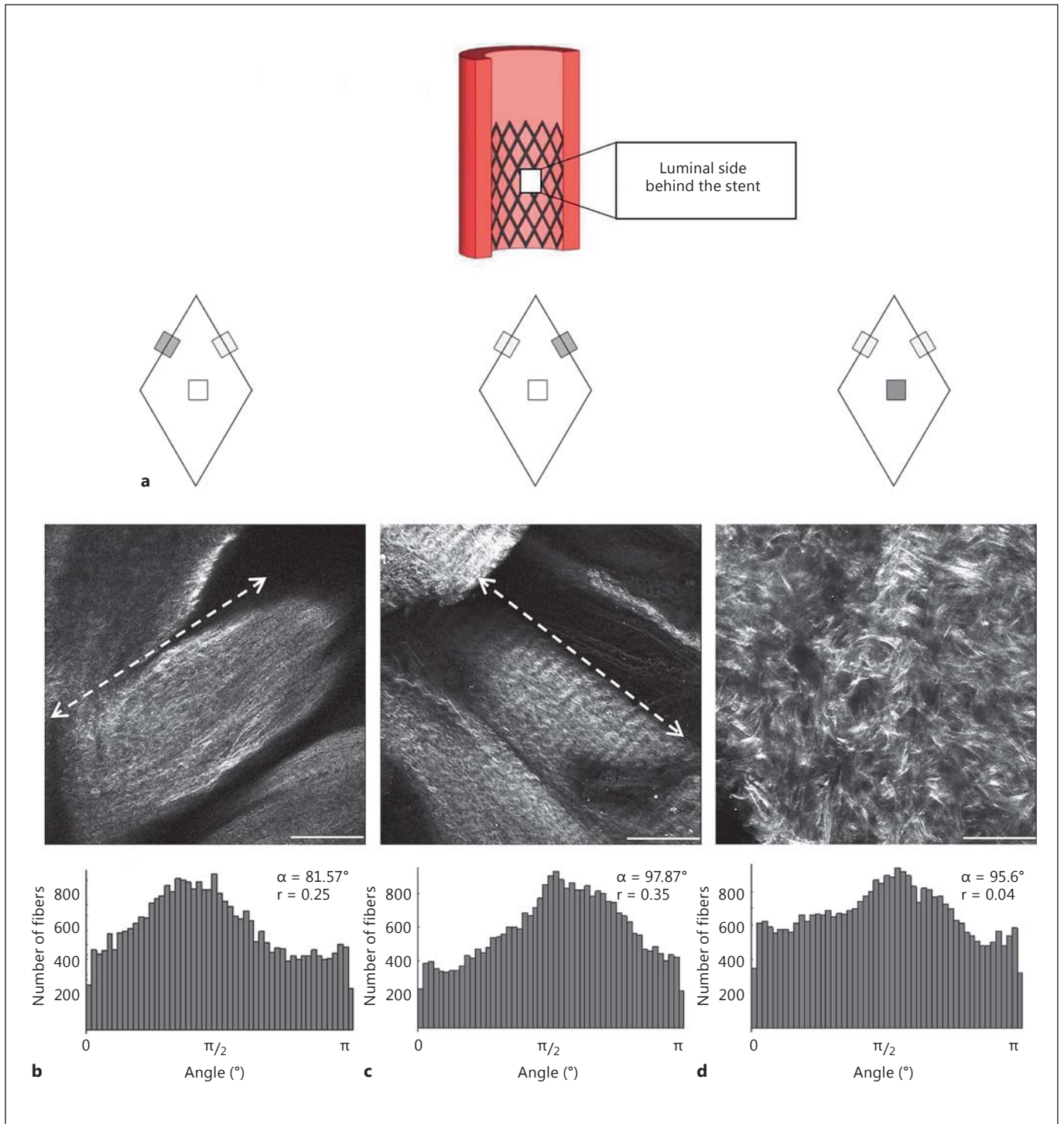
Fig. 2. Schematic representation of the region of study and three different regions of the arterial lumen behind the stent (**a**), and representative SHG images and their corresponding histograms (**b–d**). Dashed arrows in **b** and **c** show the location of the stent. Scale bars = 200 μm.

Collagen and Elastin Content

Native pulmonary artery segments from 2 different locations behind the stent and distal to the stent (n = 3 per location per sheep) were analyzed for the amount of collagen and elastin using biochemical assays. The hydroxyproline amount per dry weight, as an indicator of collagen quantity, was determined using a modification of the assay protocol described by Huszar et al. [1980]. Standard curves were prepared from rans-4-hydroxyproline (Sigma). The assay was performed after digestion of lyophilized samples in papain solution (11 mM phosphate buffer, pH = 6.5, 5 mM L-cysteine, 5 mM EDTA and 125–140 μg papain per ml) at 60°C for 16 h. For determination of the soluble elastin content, a Fastin elastin assay kit (kit F2000; Biocolor, Carrickfergus, UK) was used [Hoerstrup et al., 2002; Joddar and Ramamurthi, 2006; Baiguera et al., 2012]. Oxalic acid (0.25 m) was added to the wet samples followed by heating for 1 h at 98°C. After centrifugation, the supernatant was collected and the sediment underwent the same procedure with oxalic acid two more times. The elastin concentration in the supernatant was measured using the kit description, and the total elastin amount per wet weight was calculated from a standard curve obtained using five concentrations of α-elastin.

Statistical Analysis

Linear regression analysis was applied to evaluate potential trends in the amount of collagen and elastin as well as collagen orientation and dispersity with time. Significant deviations of the slope of the regression line from zero were evaluated. Moreover, Student's t test was performed to compare the collagen tortuosity data. $p < 0.05$ was considered as the level of significance. Statistical analyses were performed using GraphPad Prism 5 software.

Results

Collagen Fiber Orientation

In general, collagen fiber orientation changed with location in the samples, but not with implantation time between 8 and 24 weeks. Therefore, to keep consistency, collagen images obtained from samples explanted after 24 weeks are shown as representative images (fig. 2–5). Moreover, all collagen orientation data of different arterial regions of all explants are presented in figure 6.

Behind the Stent

The arterial tissues located behind the stent were analyzed in three different regions on the luminal side, as shown schematically in figure 2a. Here, collagen fibers in the vicinity of the struts were consistently aligned along the direction of the struts (fig. 2b, c), whereas between the struts, fibers were randomly oriented (fig. 2d). In all samples, collagen fiber orientation did not change with the depth of the tissue on the luminal side of the artery. On the adventitial side of the artery and behind the stent, collagen fiber orientation was influenced by the stent to different degrees in the various explants (fig. 3). At all time

points, there were some regions in which the stent showed severe penetration throughout the arterial wall, with a consequent impact on the collagen fiber alignment as a function of tissue depth (0, 10 and 20 μm; fig. 3b–d). However, in another sample, where the stent caused less penetration to the arterial lumen, no change in collagen fiber alignment was observed with tissue depth (0, 10 and 20 μm; fig. 3e–g). Results showed that on the adventitial side of the artery, the fibers were wavy and collagen orientation was mainly in the circumferential direction in both severe and less severe stent penetration cases (fig. 3b, e). On the other hand, deeper in the tissue the fibers became less wavy. Here the alignment of collagen changed toward the direction of the struts in the case of severe stent penetration, where the stent-induced collagen fiber orientation was visible up to a depth of 100 μm from the adventitial side (fig. 3c, d). However, the alignment of collagen fibers stayed circumferential when the stent penetration was less severe (fig. 3f, g) and stent-induced collagen fiber orientation was not visible at a depth of 100 μm from the adventitial side.

Immediately Distal to the Stent

The collagen orientation in the regions immediately above the stent changed dramatically toward the axial direction on both the luminal (fig. 4a, b) and the adventitial (fig. 4c, d) sides of the artery in all the explants.

Remote Control Tissue

In the region far distal to the stent, wavy fibers were mainly aligned in the circumferential direction in the outer adventitia (fig. 5a), while the main fiber orientation did not change with depth in the tissue (up to 100 μm). We did not observe any fibrous type of collagen on the luminal side of the control tissue (fig. 5b). Most likely, collagen type IV in the basal lamina was what we observed with SHG microscopy.

The mean angle data of the different regions of the arteries (n = 3 per region per sheep), except for the luminal side behind the stent and between the struts (because of the random fiber orientation or very low r value) and luminal side distal to stent (as no fibrous collagen was imaged), are shown in figure 6. For all regions except the luminal side immediately distal to the stent, the slopes of the regression line applied to the mean angle data versus time were slightly, but not significantly, positive. Furthermore, collagen orientation dispersity did not change with time either (see online suppl. fig. 1; for all online suppl. material, see www.karger.com/doi/10.1159/000442521).
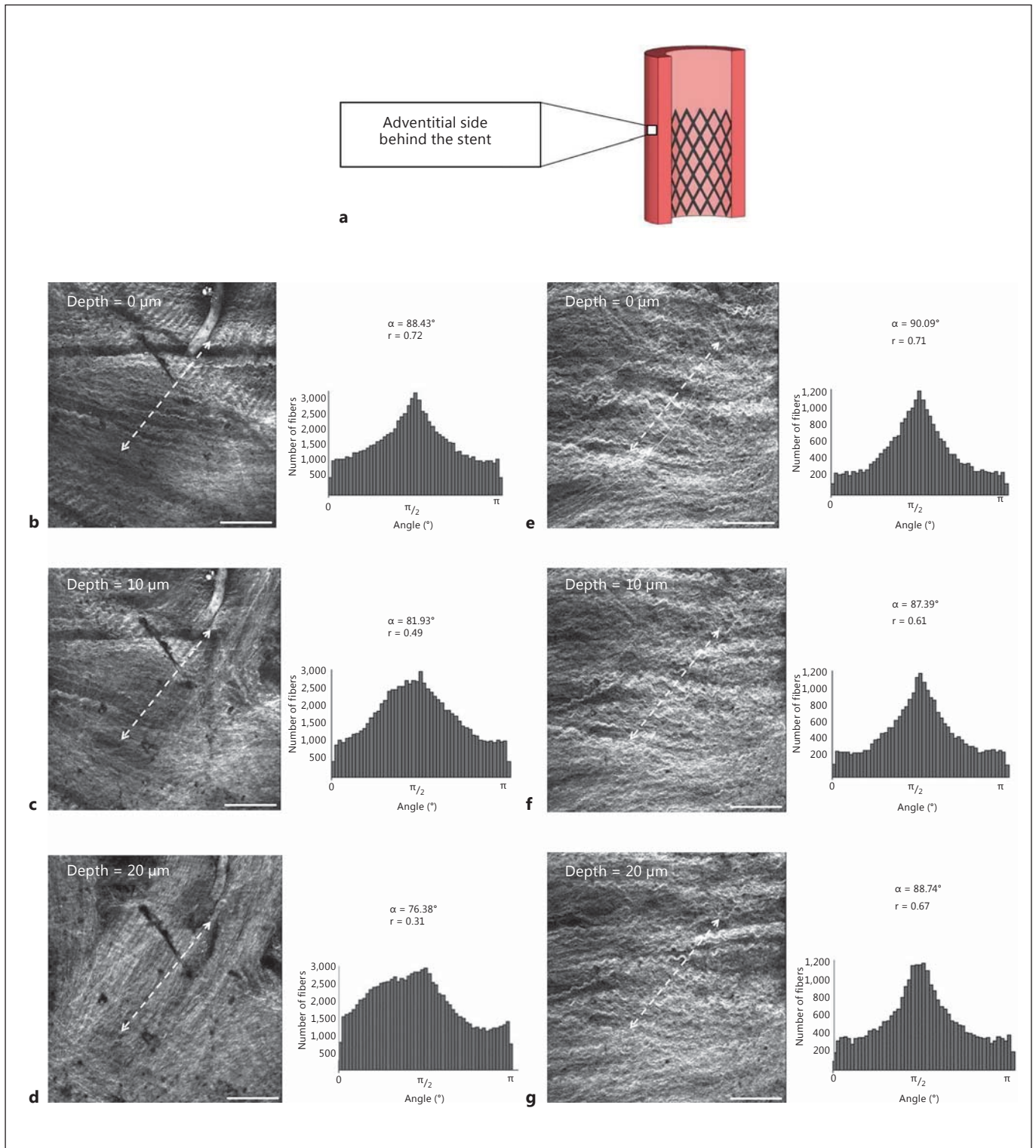
Fig. 3. Schematic representative of the region located behind the stent and adventitial side of the artery (**a**), SHG images and collagen orientation quantification histograms of 2 different arteries through the arterial thickness at an imaging depth of 0 (**b**, **e**), 10 (**c**, **f**) and 20 μm (**d**, **g**). Dashed arrows represent where the stent was located. Scale bars = 200 μm.
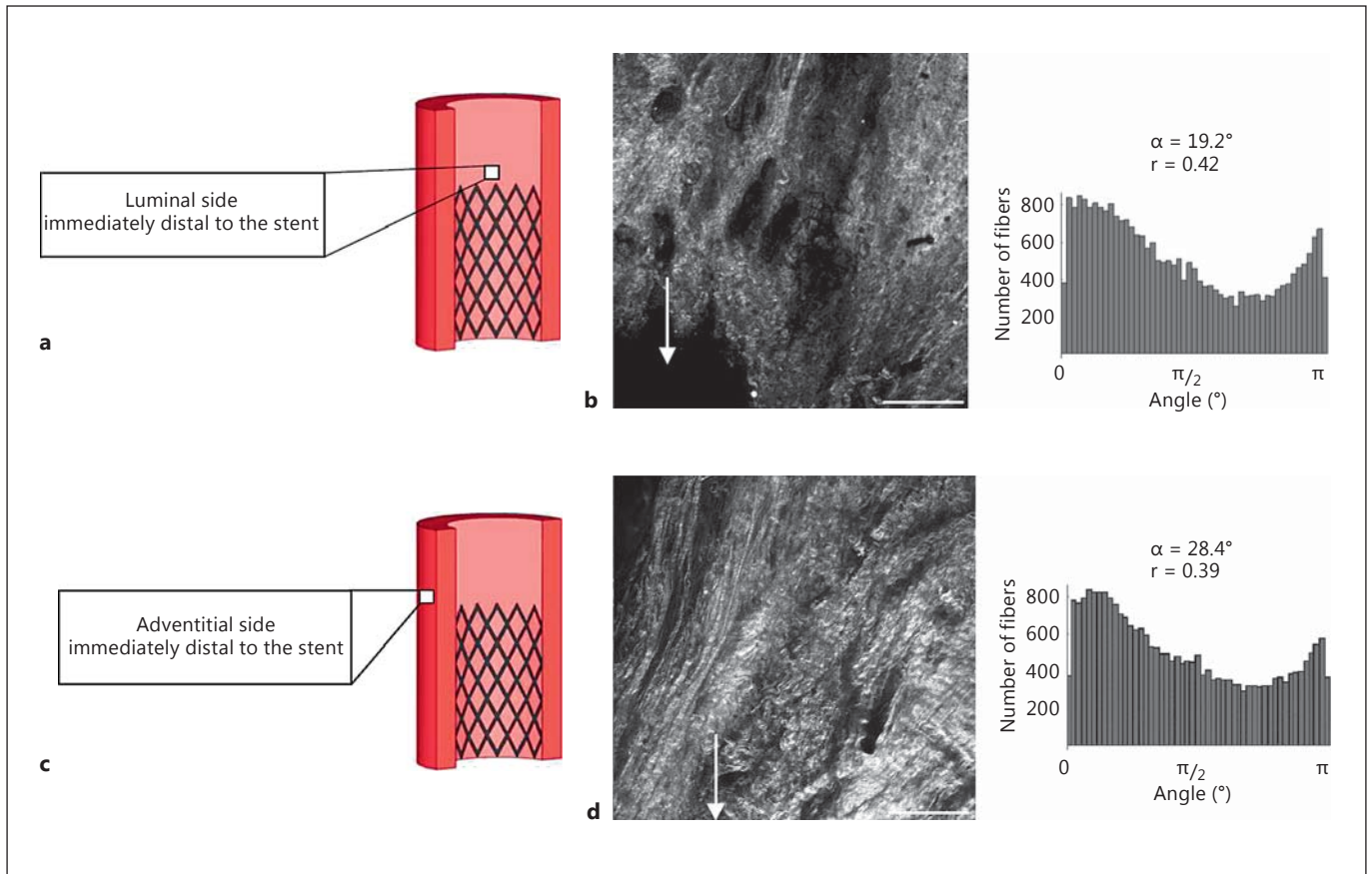
Fig. 4. Schematic view (**a**, **c**), representative SHG images and corresponding histograms (**b**, **d**) of the arterial wall lumen (**a**, **b**) and adventitia (**c**, **d**) located immediately distal to the stent. White arrows indicate where a stent strut was located. Scale bars = 200 μm.

The tortuosity index in the native vascular walls located behind the stent was 0.70 ± 0.03 [Ghazanfari et al., 2015a]. The tortuosity index of the native vascular wall located distal to the stent using the same method was 0.75 ± 0.01, which was significantly different (Student's t test, p < 0.05) from the tortuosity index corresponding to the vascular wall region behind the stent. These results indicate that collagen fibers were more undulated in the control/unloaded regions as compared to the stented/loaded regions.

Collagen and Elastin Content
The hydroxyproline and elastin amount of the arterial wall behind the stent and distal to the stent with implantation time was obtained (fig. 7). For comparison purposes, we considered the tissue distal to the stent to be representative of the original native pulmonary artery or the control tissue, and behind the stent to be representa-

tive of the stented pulmonary artery. The slope of the regression line fitted to both collagen and elastin data revealed no significance from zero.

Discussion

In the current study, we evaluated the effect of mechanical loading induced by a valved stent on collagen alignment as well as elastin and collagen content of the ovine pulmonary artery. Based on the number of samples analyzed in our study, statistically sound conclusions are difficult to make. Yet, our study provides initial new insights into in vivo arterial wall remodeling after minimally invasive heart valve implantation, which show stent-induced local changes in ECM over a period of 6 months. It should be realized that it is logistically and financially unrealistic to perform large numbers of experiments in
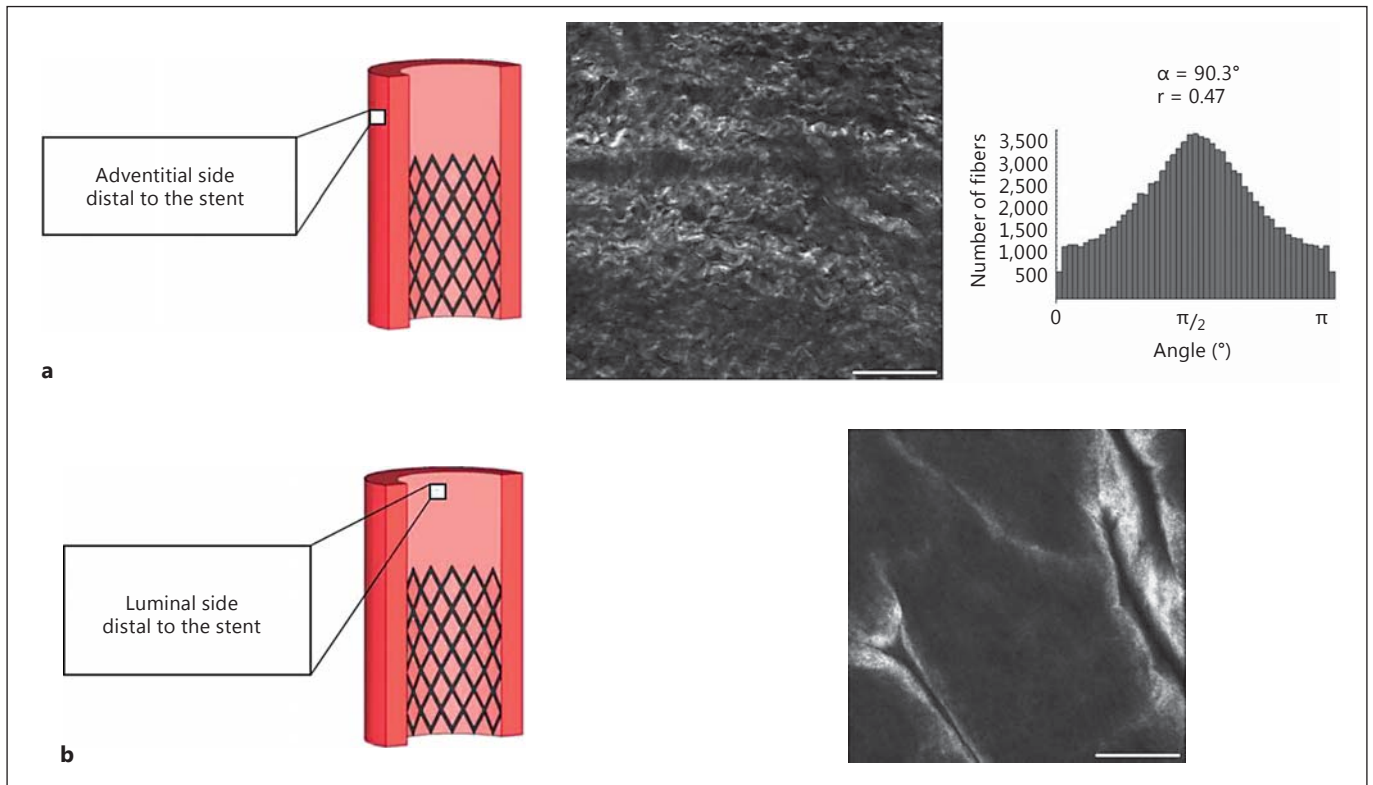
Fig. 5. Schematic drawing, representative SHG images and corresponding histogram of the arterial adventitia (**a**) and lumen (**b**) located distal to the stent. No histogram is included in **b** as no fibrous collagen was visualized. Scale bars = 200 μm.
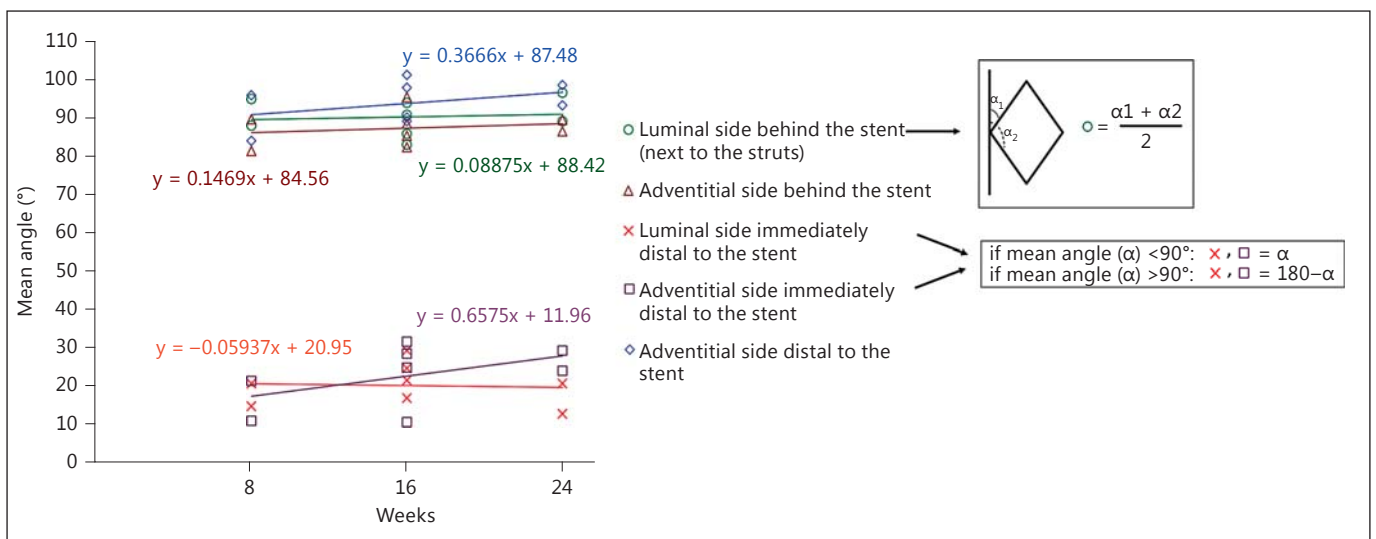
Fig. 6. The mean angle of collagen fiber orientation of different arterial regions, except for the luminal side behind the stent and between struts (because of the random fiber orientation or very low r value) and the luminal side distal to stent (as no fibrous collagen was imaged). The mean angle values of collagen fibers (○) behind two adjacent struts were averaged and presented as one value. Moreover, to present the axial alignment of fibers, mean fiber angles larger than 90° were deducted from 180° for regions immediately distal to the stent (×,□). The slope of the regression line showed no significant deviation from zero.

Ghazanfari/Driessen-Mol/Hoerstrup/
Baaijens/Bouten
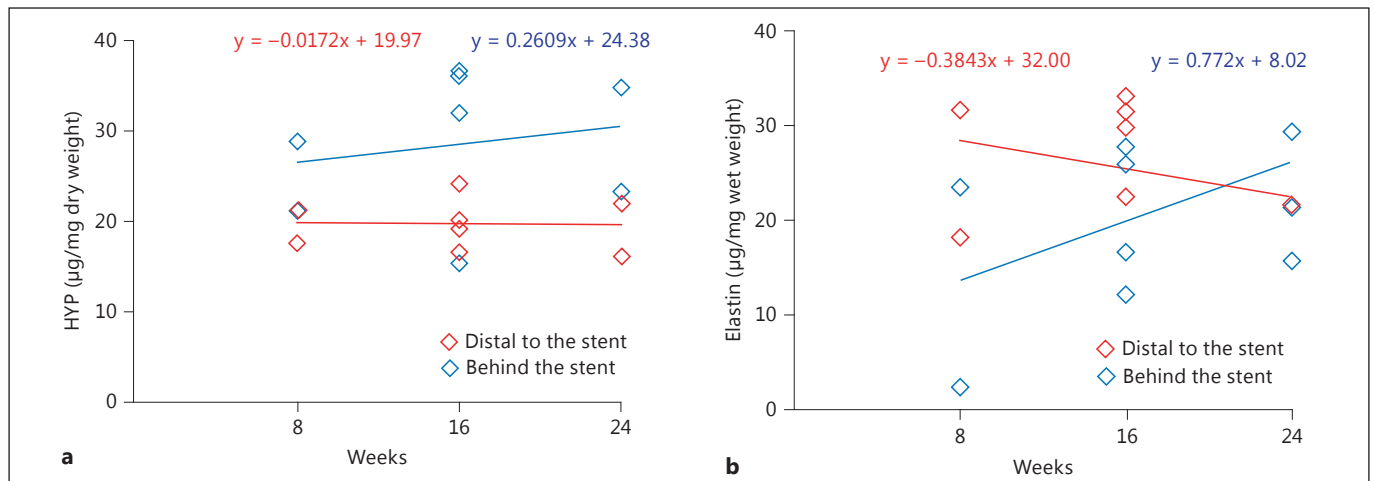
Fig. 7. Elastin (**a**) and collagen (**b**) content of the regions located behind and distal to the stented area. The slope of the regression line revealed no significant deviation from zero. HYP = Hydroxyproline.

large animals for a long period of time. Therefore, future studies, for example in other model systems, are needed to fully understand the collagen remodeling process in vivo.

SHG images showed no changes in collagen orientation in the remote vascular wall (~5 cm distal to the stent) following the stenting procedure. At this location, collagen fibers were circumferentially orientated in the adventitia of the arteries, similar to what was observed by Fata et al. [2013] for untreated healthy adult ovine pulmonary arteries. Likewise, the lack of fibrous collagen at the luminal side of the artery, distal to the stent region, corresponds to the findings of Fata et al. [2013], who showed a dense elastin network on the luminal side of (nonstented) adult ovine pulmonary arteries which became more sparse toward the adventitia. Considering the consistency between the data of Fata et al. [2013] and the observations on the remote tissue in our study, the use of the remote tissue as the control tissue for ECM remodeling seems admissible.

The stented part of the artery, however, displayed regional differences in collagen organization on both the luminal and adventitial sides, independent of the implantation time. On the adventitial side, undulated collagen fibers changed drastically and rapidly (within 8 weeks) from a mainly circumferential direction distal to the stent (~5 cm) to an axial direction immediately above the stent. This axial alignment might be an indication of a compliance mismatch between the stented and the adjacent non-stented regions. Behind the stent, fibers were again observed to be circumferentially oriented, but more straightened due to the expansion of the stent. By expansion of the artery, collagen fibers gradually start to engage in the carrying load and provide the tissue the ability to prevent overexpansion. It has been shown that collagen fibers were more undulated in the unloaded arteries [Clark and Glagov, 1985; Dingemans et al., 2000] compared to their loaded counterparts [Canham et al., 1989; Rezakhaniha et al., 2012; Schrauwen et al., 2012].

On the luminal side of the stented artery, where the presence of the stent is expected to induce higher tissue stresses and strains, but perhaps also local vascular trauma, a combination of biophysical cues seems to trigger stent-induced tissue remodeling. The alignment of collagen fibers along the stent struts is hypothesized to be caused by the mechanism of contact guidance. Engelmayr et al. [2006] exhibited how collagen alignment was guided by large-scale diamond-shaped scaffolds. Large-scale scaffolds with a grid of 200-mm-wide rectangular pores showed a great capacity to guide collagen alignment parallel to the strut long-axis in the vicinity of the struts. The authors concluded that due to contact guidance the collagen fibers attached uniformly along the scaffold struts. This mechanism was evidenced in vitro, and in the current study it was shown that the same mechanism is involved in the in vivo situation. On the other hand, we performed biochemical analyses and compared the outcomes of the control (distal to the stent) and stented ovine pulmonary tissues. The trend of collagen and elastin amount did not change with time, which could be an in-

dication of the stable tissue matrix. Thus, mechanically induced structural remodeling showed physiological adaptation toward a mechanically functional tissue.

High strains and stresses induced by the stent can lead to vascular complications. For the optimum stent design, the interaction between the stent and arterial wall should be studied. Reported results on estimated stress and strain applied to the arteries by the stent are limited to the numerical studies as it is difficult to measure these parameters under physiological conditions [Holzapfel et al., 2005; Kiousis et al., 2007]. Furthermore, it has been shown that mechanical properties of the arterial root play an important role in the long-term functionality of the valves [De Hart et al., 2003]. Thus, fiber characteristics data can be used as inputs for numerical models to calculate the stress and strain applied to the tissue and to predict local tissue biomechanics.

In conclusion, collagen orientation changes in ovine native pulmonary arteries in response to the stenting procedure were evaluated. The results showed that fibers became straightened on the adventitial side of the artery due to the arterial expansion. SHG microscopy revealed that the collagen organization at the luminal side of the artery and in direct contact with the stent was dramatically changed, while collagen and elastin content did not change due to the stenting. This study has shown that vascular collagen remodeling induced by the stent occurred early (before 8 weeks) and did not change with time, indicating stable remodeling, at least up to 24 weeks. However, due to the limited sample size at two time points, future studies are needed to fully elucidate the remodeling process.

References

Baiguera, S., C. Del Gaudio, M.O. Jaus, L. Polizzi, A. Gonfiotti, C.E. Comin, A. Bianco, D. Ribatti, D.A. Taylor, P. Macchiarini (2012) Long-term changes to in vitro preserved bioengineered human trachea and their implications for decellularized tissues. Biomaterials 33: 3662–3672.

Bailey, A.J., R.G. Paul, L. Knott (1998) Mechanisms of maturation and ageing of collagen. Mech Ageing Dev 106: 1–56.

Campagnola, P.J., A.C. Millard, M. Terasaki, P.E. Hoppe, C.J. Malone, W.A. Mohler (2002) Three-dimensional high-resolution second-harmonic generation imaging of endogenous structural proteins in biological tissues. Biophys J 82: 493–508.

Canham, P.B., H.M. Finlay, J.G. Dixon, D.R. Boughner, A. Chen (1989) Measurements from light and polarised light microscophy of human arteries fixed at distending pressure. Cardiovasc Res 23: 973–982.

Chung, I.M., H.K. Gold, S.M. Schwartz, Y. Ikari, M.A. Reidy, T.N. Wight (2002) Enhanced extracellular matrix accumulation in restenosis of coronary arteries after stent deployment. J Am Coll Cardiol 40: 2072–2081.

Clark, J.M., S. Glagov (1985) Transmural organization of the arterial media: the lamellar unit revisited. Arteriosclerosis 5: 19–34.

Daniels, F., B.M. Ter Haar Romeny, M.P. Rubbens, H. van Assen (2006) Quantification of collagen orientation in 3D engineered tissue. IFMBE Proc 15: 282–286.

De Hart, J., F.P. Baaijens, G.W. Peters, P.J. Schreurs (2003) A computational fluid-structure interaction analysis of a fiber-reinforced stentless aortic valve. J Biomech 36: 699–712.

Dingemans, K.P., P. Teeling, J.H. Lagendijk, A.E. Becker (2000) Extracellular matrix of the human aortic media: an ultrastructural histochemical and immunohistochemical study of the adult aortic media. Anat Rec 258: 1–14.

Dobrin, P.B. (1978) Mechanical properties of arteries. Physiol Rev 58: 397–460.

Engelmayr Jr., G.C., G.D. Papworth, S.C. Watkins, J.E. Mayer Jr., M.S. Sacks (2006) Guidance of engineered tissue collagen orientation by large-scale scaffold microstructures. J Biomech 39: 1819–1831.

Eyden, B., M. Tzaphlidou (2001) Structural variations of collagen in normal and pathological tissues: role of electron microscopy. Micron 32: 287–300.

Fata, B., C.A. Carruthers, G. Gibson, S.C. Watkins, D. Gottlieb, J.E. Mayer, M.S. Sacks (2013) Regional structural and biomechanical alterations of the ovine main pulmonary artery during postnatal growth. J Biomech Eng 135: 021022.

Georgiou, E., T. Theodossiou, V. Hovhannisya, K. Politopoulos, G.S. Rapti, D. Yova (2000) Second and third optical harmonic generation in type I collagen, by nanosecond laser irradiation, over a broad spectral region. Opt Commun 176: 253–260.

Ghazanfari, S., A. Driessen Mol, B. Sanders, P.E. Dijkman, S.P. Hoerstrup, F.P.T. Baaijens, C.V.C. Bouten (2015a) Evolution of in vivo collagen remodeling and maturation in the vascular wall of decellularized stented tissue engineered heart valves. Tissue Engineering Part A 21: 2206–2215.

Ghazanfari, S., A. Driessen-Mol, G.J. Strijkers, F.P.T. Baaijens, C.V.C. Bouten (2015b) The evolution of collagen fiber orientation in engineered cardiovascular tissues visualized by diffusion tensor imaging. PLoS One 10: e0127847.

Ghazanfari, S., A. Driessen-Mol, G.J. Strijkers, F.M.W. Kanters, F.P.T. Baaijens, C.V.C. Bouten (2012) A comparative analysis of the collagen architecture in the carotid artery: second harmonic generation versus diffusion tensor imaging. Biochemic Biophys Res Commun 426: 54–58.

Hammermeister, K., G.K. Sethi, W.G. Henderson, F.L. Grover, C. Oprian, S.H. Rahimtoola (2000) Outcomes 15 years after valve replacement with a mechanical versus a bioprosthetic valve: final report of the Veterans Affairs Randomized Trial. J Am Coll Cardiol 36: 1152–1158.

Hoerstrup, S.P., A. Kadner, C. Breymann, C.F. Maurus, C.I. Guenter, R. Sodian, J.F. Visjager, G. Zund, M.I. Turina (2002) Living, autologous pulmonary artery conduits tissue engineered from human umbilical cord cells. Ann Thorac Surg 74: 46–52.

Hoerstrup, S.P., R. Sodian, S. Daebritz, J. Wang, E.A. Bacha, D.P. Martin, A.M. Moran, K.J. Guleserian, J.S. Sperling, S. Kaushal, J.P. Vacanti, F.J. Schoen, J.E. Mayer Jr. (2000) Functional living trileaflet heart valves grown in vitro. Circulation *102:* 44–49.

Holzapfel, G.A., M. Stadler, T.C. Gasser (2005) Changes in the mechanical environment of stenotic arteries during interaction with stents: computational assessment of parametric stent designs. J Biomech Eng *127:* 166–180.

Huszar, G., J. Maiocco, F. Naftolin (1980) Monitoring of collagen and collagen fragments in chromatography of protein mixtures. Anal Biochem *105:* 424–429.

James, V.J., L. Delbridge, S.V. McLennan, D.K. Yue (1991) Use of x-ray diffraction in study of human diabetic and aging collagen. Diabetes *40:* 391–394.

Joddar, B., A. Ramamurthi (2006) Elastogenic effects of exogenous hyaluronan oligosaccharides on vascular smooth muscle cells. Biomaterials *27:* 5698–5707.

Kiousis, D.E., T.C. Gasser, G.A. Holzapfel (2007) A numerical model to study the interaction of vascular stents with human atherosclerotic lesions. Ann Biomed Eng *35:* 1857–1869.

Mol, A., N.J. Driessen, M.C. Rutten, S.P. Hoerstrup, C.V. Bouten, F.P. Baaijens (2005a) Tissue engineering of human heart valve leaflets: a novel bioreactor for a strain-based conditioning approach. Ann Biomed Eng *33:* 1778–1788.

Mol, A., M.I. van Lieshout, C.G. Dam-de Veen, S. Neuenschwander, S.P. Hoerstrup, F.P. Baaijens, C.V. Bouten (2005b) Fibrin as a cell carrier in cardiovascular tissue engineering applications. Biomaterials *2616:* 3113–3121.

Post, M.J., C. Borst, R.E. Kuntz (1994) The relative importance of arterial remodeling compared with intimal hyperplasia in lumen renarrowing after balloon angioplasty: a study in the normal rabbit and the hypercholesterolemic Yucatan micropig. Circulation *89:* 2816–2821.

Rezakhaniha, R., A. Agianniotis, J.T.C. Schrauwen, A. Griffa, D. Sage, C.V. Bouten, F.N. van de Vosse, M. Unser, N. Stergiopulos (2012) Experimental investigation of collagen waviness and orientation in the arterial adventitia using confocal laser scanning microscopy. Biomech Model Mechanobiol *11:* 461–473.

Rogers, C., D.Y. Tseng, J.C. Squire, E.R. Edelman (1999) Balloon-artery interactions during stent placement: a finite element analysis approach to pressure, compliance, and stent design as contributors to vascular injury. Circ Res *84:* 378–383.

Rubbens, M.P., A. Driessen-Mol, R.A. Boerboom, M.M. Koppert, H.C. van Assen, B.M. TerHaar Romeny, F.P. Baaijens, C.V. Bouten (2009) Quantification of the temporal evolution of collagen orientation in mechanically conditioned engineered cardiovascular tissues. Ann Biomed Eng *37:* 1263–1272.

Schmidt, D., P.E. Dijkman, A. Driessen-Mol, R. Stenger, C. Mariani, A. Puolakka, M. Rissanen, T. Deichmann, A. Odermatt, B. Weber, M.Y. Emmert, G. Zund, F.P. Baaijens, S.P. Hoerstrup (2010) Minimally-invasive implantation of living tissue engineered heart valves: a comprehensive approach from autologous vascular cells to stem cells. J Am Coll Cardiol *56:* 510–520.

Schrauwen, J.T.C., A. Vilanova, R. Rezakhaniha, N. Stergiopulos, F.N. van de Vosse, P.H.M. Bovendeerd (2012) A method for the quantification of the pressure dependent 3D collagen configuration in the arterial adventitia. J Struct Biol *180:* 335–342.

Spina, M., F. Ortolani, A. El Messlemani, A. Gandaglia, J. Bujan, N. Garcia-Honduvilla, I. Vesely, G. Gerosa, D. Casarotto, L. Petrelli, M. Marchini (2003) Isolation of intact aortic valve scaffolds for heart-valve bioprostheses: extracellular matrix structure, prevention from calcification, and cell repopulation features. J Biomed Mater Res A *67:* 1338–1350.

Steed, D.L. (1997) The role of growth factors in wound healing. Surg Clin North Am *77:* 575–586.

Strupler, M., A.M. Pena, M. Hernest, P.L. Tharaux, J.L. Martin, E. Beaurepaire, M.C. Schanne-Klein (2007) Second harmonic imaging and scoring of collagen in fibrotic tissues. Optics Express *15:* 4054–4065.

Sun, J.C., M.J. Davidson, A. Lamy, J.W. Eikelboom (2009) Antithrombotic management of patients with prosthetic heart valves: current evidence and future trends. Lancet *374:* 565–576.

van Vlimmeren, M.A., A. Driessen-Mol, C.W.J. Oomens, F.P.T. Baaijens (2011) An in vitro model system to quantify stress generation, compaction, and retraction in engineered heart valve tissue. Tissue Eng Part C Methods *17:* 983–991.

Willfort-Ehringer, A., R. Ahmadi, D. Gruber, M.E. Gschwandtner, A. Haumer, M. Haumer, H. Ehringer (2004) Arterial remodeling and hemodynamics in carotid stents: a prospective duplex ultrasound study over 2 years. J Vasc Surg *39:* 728–734.

Yacoub, M.H., J.J.M. Takkenberg (2005) Will heart valve tissue engineering change the world? Nat Clin Pract Cardiovasc Med *2:* 60–61.

Ye, X., Q. Zhao, X. Sun, H. Li (2009) Enhancement of mesenchymal stem cell attachment to decellularized porcine aortic valve scaffold by in vitro coating with antibody against CD90: a preliminary study on antibody-modified tissue-engineered heart valve. Tissue Eng Part A *15:* 1–11.

Zipfel, W.R., R.M. Williams, R. Christie, A.Y. Nikitin, B.T. Hyman, W.W. Webb (2003) Live tissue intrinsic emission microscopy using multiphoton-excited native fluorescence and second harmonic generation. Proc Natl Acad Sci USA *12:* 7075–7080.